The long-ranged Potts model revisited: a multicanonical approach

Sylvain Reynal, Hung-The Diep

The long-ranged Potts model revisited: a multicanonical approach

S. Reynal* and H.T.Diep
Laboratoire de Physique Théorique et Modélisation,
CNRS-Université de Cergy-Pontoise, 5 mail Gay-Lussac,
Neuville sur Oise, 95031 Cergy-Pontoise Cedex, France

We investigate the critical behavior of the one-dimensional q-state Potts model with long-ranged (LR) interaction $1/r^{d+\sigma}$, using a multicanonical algorithm. The recursion scheme initially proposed by Berg is improved so as to make it suitable for a large class of LR models with unequally spaced out energy levels. The choice of an efficient predictor and a reliable convergence criterion is discussed. We obtain transition temperatures in the first-order regime which are in far better agreement with mean-field predictions than in any previous study. By relying on the location of spinodal points and resorting to scaling arguments, we determine the threshold value $\sigma_c(q)$ separating the first- and second-order regime to an unprecedented two digit precision within the range $3 \leq q \leq 9$. We offer convincing numerical evidence supporting $\sigma_c(q) < 1.0$ for all q, by virtue of an unusual finite-size effect which has not been noticed before, namely finite-size scaling predicts a second-order transition in the thermodynamic limit, despite the first-order nature of transitions at finite size. A qualitative account in terms of correlation lengths is provided. Finally, we find the cross-over between LR and short-range regimes to occur inside a narrow window $1.0 < \sigma < 1.2$, thus lending strong support to Sak's scenario.

PACS numbers: 05.10.Ln, 64.60.Cn, 75.10.Hk

I. INTRODUCTION

Microscopic models with long-ranged (LR) interactions decaying as a power law, *i.e.* as $1/r^{d+\sigma}$, have aroused renewed interest during the last decade. Beyond their fundamental relevance for the understanding of critical phenomena, they have started playing a seminal role in the modeling of neural networks [1] and spin glasses with RKKY interactions [2], systems undergoing phase separation, e.g. highly ionic systems [3] and model alloys [4], and more widely a large class of chemical or biological models where electrostatic interactions, polarization or van der Waals forces play a central role. They have also attracted much attention in the framework of nonextensive thermodynamics, where a possible equivalence with short-ranged (SR) models is within consideration [5].

Since the very early work of Ruelle [6], LR spin models in particular have been extensively studied. In one dimensional models, it has been widely proven that long-range order occurs at finite temperature if and only if $\sigma \leq 1$ [6–10], and this comes in strong contrast with the (SR) case where no phase transition exists at finite temperature. Fisher and coworkers [11] have shown that the upper critical dimension is reduced to $d^* = 2\sigma$, whereby one-dimensional LR models exhibit mean-field like behavior for $\sigma < 0.5$, with critical exponents assuming their classical values $\nu = 1/\sigma$ and $\gamma = 1$ provided the phase transition is continuous. Conversely, the critical behavior for $\sigma \geq 0.5$ yields non-trivial exponents, and LR models in effect go through a variety of universality classes as σ is varied within this range, thus exhibiting rich critical behavior. Due to the ability to continuously vary the range of interaction, which in effect alters the effective dimension of the model, one-dimensional LR models are therefore a powerful paradigm for studying the dependence of critical properties on dimensionality, e.g. in systems above their upper critical dimension [12].

While significant emphasis has been put on the Ising chain (see e.g. [13] for a review), specific studies of the LR q-state Potts model are less numerous and rather recent. These include transfer matrix studies combined with Finite Range Scaling (FRS) [14], RG analysis based on Wilson's momentum-shell method [15] or a real-space procedure [16, 17], and Monte-Carlo (MC) simulations [18–24]. The latter, however, mostly focused on the case $q = 3$, and led to numerical estimates of critical exponents and temperatures showing some discrepancies. Due to the higher ground-state degeneracy, this model reveals a phase diagram being markedly richer than that of the Ising chain. It has been shown in the SR case that the transition changes from a continuous to a first-order one as the number of states q is increased beyond a threshold value $q_c(d)$ depending on the dimensionality of the model. For instance, $q_c(2) = 4$ and $q_c(4) = 2$ [25, 26] (see also Ref. [27] for a complete review). As of the LR case in $d = 1$, Glumac and Uzelac have shown from MC studies of the three- and five-state Potts model [18] that the same sort of behavior occurs, *i.e.* there is a so-called tricritical point at some value $\sigma_c(q)$ depending on q, and the transition is continuous for $\sigma > \sigma_c$. This qualitative picture was later reinforced in [20] for $q = 3, 5, 7, 9$ and in [23] for $q = 3$, both relying on MC studies, and in [19] using a graph-weights approach. On the other hand, it is noteworthy that traditional RG analysis usually do not distinguish between first- and second-order

*Electronic address: reynal@ensea.fr; URL: http://www.ensea.fr/staff/reynal; Permanent address: E.N.S.E.A., 6 av. du Ponceau, 95014 Cergy Cedex, France.

transition, hence hardly give any hint here [17].

Although it is now believed that q_c depends continuously on the range of interaction for this class of model, the exact location of the tricritical line separating both regions is still fairly controversial. The biggest hurdle for a precise and reliable determination of this borderline actually stems from the weakening of the discontinuous transition as σ_c is approached, however exceptionally large lattice size may be used, e.g. using the efficient Luijten-Blöte cluster algorithm [28]. While for $q = 3$, σ_c was claimed to lie between 0.6 and 0.7 in [18], Krech and Luijten pointed out that $\sigma = 0.7$ still belongs to the first-order regime, and that the second-order regime may set in for $\sigma = 0.75$ only [23]. The situation with $q = 5$ turns out to be even worse, with numerical estimates available only within fairly large ranges: a lower boundary value of 0.8 was reported in [18], whereas $0.7 < \sigma_c(5) < 1.0$ according to [20]. These results have not yielded a very precise phase diagram as yet, with the only reliable assertion being that $\sigma_c(q)$ increases with q.

The marginal case $\sigma = 1$ raises another set of thorny questions: in [20] it was reported that the onset of a first-order transition occurred for $q \geq 9$, yet Cardy has shown in [16] that inverse square interactions yield a KT-like transition, *i.e.* governed by topological defects [29], an assumption which is incompatible with a first-order transition. While the work of Luijten and Messingfeld on the three-state Potts model [24] lends further support to Cardy's assertion, the controversy appears still unsettled, and in this view a determination of the asymptotic behavior of $\sigma_c(q)$ as $q \to \infty$ seems of major interest indeed.

We wish to shed new light on some of these contradictory results using MC simulations in generalized ensembles, with particular emphasis given to the first-order regime. The aim of this work is thus twofold. First, we propose an implementation of the multicanonical algorithm dedicated to the numerical study of LR models. This algorithm, devised by Berg and Neuhaus a decade ago [30, 31], has been successfully applied in the past to SR models undergoing first-order transitions. As numerical studies of models exhibiting first-order transitions are dramatically hampered by huge tunneling times when using standard Metropolis move-updates [32, 33], a multicanonical approach is indeed an appropriate choice for both the determination of the location of the tricritical line and the estimation of critical couplings in the first-order region $\sigma < \sigma_c$. Our purpose is therefore to adapt the scheme initially proposed for SR models so as to make it suitable for a large class of LR models. Secondly, by relying on an extensive study for $3 \leq q \leq 9$ and a wide range of σ values, we bring convincing conclusions regarding the location of the tricritical line, the range of validity of the mean-field-like behavior, which we find much larger than in previous studies, and the cross-over from the LR to the SR regime, although the latter was investigated for the three-state model only. We show that our multicanonical implementation yields numerical estimates which are in agreement with and often better than those found in previous studies, although our simulations were performed by relying on medium lattice sizes, *i.e.* $L \leq 400$ spins. In particular, we obtain the following estimates for $\sigma_c(q)$: $\sigma(3) = 0.72(1)$,$\sigma(5) = 0.88(2)$, $\sigma(7) = 0.94(2)$ and $\sigma(9) = 0.965(20)$, and this results indeed are of unprecedented precision. We also offer convincing evidence that the phase transition in the limiting case $\sigma = 1.0$ is not of the first-order for all values of q, by virtue of an unusual finite-size effect which has not been noticed before. A detailed FSS analysis conducted for $q = 9$ shows that, while the transition belongs to the first-order regime at finite lattice size, its first-order nature wanes sufficiently as size is increased so that the transition tends to a second-order one in the thermodynamic limit. We give a qualitative account of this behavior in terms of correlation lengths, and by raising some open questions regarding the dynamics of first-order transitions in the LR case, we try to challenge the usual picture inherited from SR models. Finally, by relying on the shape of the specific heat and computing several moments of the magnetization, we conclude that a cross-over between LR and SR regimes occurs inside a narrow window $1.0 < \sigma < 1.2$

The layout of this article is as follows. In section II, we first review some prominent features of the LR Potts model through an MF analysis. Special emphasis is given to the calculation of the location of spinodal points, a feature we will use in section IV for estimating $\sigma_c(q)$. Section III is devoted to implementation details of the multicanonical algorithm specific to LR models. We discuss the iteration procedure used to obtain the best estimate for the density of state, the choice of an efficient predictor and a reliable convergence criterion. Improvements over the original algorithm are made in order to work out the algorithm instability due to low energy levels being unequally spaced out. Numerical results regarding both the first and the second order regime are then presented in section IV. In the absence of any previous implementation of a generalized ensemble algorithm in the case of LR spin models, we pay particular attention to comparison with other standard MC algorithms, *i.e.* in terms of dynamical exponents, tunneling times and accuracy of numerical estimates of critical couplings.

II. MODEL AND MEAN-FIELD THEORY

Throughout this work we consider a ferromagnetic Potts model incorporating LR interactions in $d = 1$. This model is derived from a generalized q-state Potts Hamiltonian, *i.e.*

$$H = -\frac{1}{2}\sum_{i \neq j} J_{ij}\delta_{\sigma_i,\sigma_j} - \sum_i h_i \delta_{\sigma_i,\sigma_0}$$

where the Potts spin σ_i at site i can take on the values $1, \ldots, q$, the first sum runs over all pairs of sites, and

h_i is an external aligning field favoring condensation in state σ_0. Incorporation of LR interaction is carried out by setting

$$J_{ij} = J(|i-j|) = \frac{1}{|i-j|^{d+\sigma}}$$

where $d = 1$ throughout this study, and σ is an adjustable parameter which can be related to the effective dimension of the model. As σ falls off to -1, this model tends to the mean-field case where all interactions have equal strength, whereas the limiting case $\sigma \to \infty$ corresponds to a pure SR model. Crossover from LR to SR behavior should actually takes place at $\sigma = 1$ [34, 35], yet no numerical evidence has been given so far for this model which would reinforce this assertion. The thermodynamics of the model is studied numerically by way of the following order parameter,

$$M = \frac{q \max_n \rho_n - 1}{q-1}$$

where $n = 1 \dots q$, and ρ_n is the density of Potts spins in state n, which varies between $1/q$ at infinite temperature and 1 in the ground state. On a finite lattice of size L, numerical implementation is carried out by using periodic boundary conditions, *i.e.* one adds up interactions between all the spins of the original lattice only, and replaces the bare coupling constant between two spins distant of r by $\tilde{J}(r) = \sum_{n=-\infty}^{+\infty} J(r+nL)$. Retaining interactions such that $|i-j| < L/2$ only leads indeed to strong shifts in energy and critical couplings for low σ values, especially when Finite Size Scaling (FSS) is to be used with medium lattice sizes. For the purpose of numerical evaluation, this sum may be re-expressed as

$$\tilde{J}(r) = \frac{1}{r^{1+\sigma}} + \frac{1}{L^{1+\sigma}} \left[\zeta\left(1+\sigma, 1+\frac{r}{L}\right) + \zeta\left(1+\sigma, 1-\frac{r}{L}\right) \right]$$

where $\zeta(s,\alpha)$ denotes the Hurwitz zeta function. The self-energy shall be omitted since it is just an additive constant to the total energy.

Mean field behavior can be readily obtained by using a variational MF approach (see for instance [36]), which relies on the minimization of the following functional

$$F[\rho] = \mathrm{Tr}\, \rho H + kT\, \mathrm{Tr}\, \rho \log \rho$$

with respect to a trial density matrix ρ. Here the trace operation means a sum over all spin configurations, and the dependence of H and ρ on the spin configuration is implied. $F[\rho]$ reaches a minimum whenever $\rho = e^{-H/kT}/Z$, *i.e.* in the case of a canonical Gibbs distribution, and this minimum yields the free energy of the system. Mean-field approximation allows us to express the density matrix ρ of the whole system as a product of one-site density matrices ρ_i which depend solely on the spin variable at site i. We may thus rewrite the trace operation as a sum involving traces on single spin variables, namely

$$F[\rho] = kT \sum_i \mathrm{Tr}_i\, \rho_i \log \rho_i - \sum_i h_i\, \mathrm{Tr}_i\, \rho_i \delta_{\sigma_i,\sigma_0} - \frac{1}{2} \sum_{i \neq j} \mathrm{Tr}_i\, \rho_i\, \mathrm{Tr}_j\, \rho_j J_{ij} \delta_{\sigma_i,\sigma_j}$$

For further comparison with numerical results, we are mainly interested in expressing the free energy as a function of an order parameter which is as similar as possible to the one defined above. This is carried out by parameterizing the trial density matrix ρ_i in terms of an order parameter field m_i defined as follow:

$$m_i = \left\langle \frac{q\delta_{\sigma_i,\sigma_0} - 1}{q-1} \right\rangle_{\rho_i}$$

where the average is weighted by the trial density matrix ρ_i. Seeing that all states but state σ_0 are equivalent, the constraint $\mathrm{Tr}\, \rho_i = 1$ thus yields

$$\rho_i(m_i, \sigma_i) = \frac{1-m_i}{q} + m_i \delta_{\sigma_i,\sigma_0}$$

Considering a uniform external field $h_i = h$, we have $m_i = m$ for all sites, hence the free-energy per spin $f(m)$ reduces to

$$\frac{qf(m)}{q-1} = -hm - \zeta(1+\sigma)m^2 + kT\{(1-m)\log(1-m) + \frac{1+m(q-1)}{q-1}\log(1+m(q-1))\} \quad (1)$$

where we dropped terms which are constant in m so that $f(0) = 0$, and $\zeta(1+\sigma)$ is the Riemann zeta function. This function expands as $1/\sigma$ around $\sigma = 0$, hence transition temperatures are expected to vary as $1/\sigma$ in the vicinity of the MF regime. Equilibrium values of the order parameter are located at minima of the free energy, and it can be seen that $m = 0$ is a stable minimum for $kT \geq 2\zeta(1+\sigma)/q$. For $q = 2$, there is no third order term in the series expansion of $f(m)$, hence a second-order transition occurs at $kT_c = \zeta(1+\sigma)$. For $q \geq 3$, the negative coefficient in the third order term of the series expansion gives birth to a second minimum, which physically corresponds to a first-order transition. At the transition temperature, the free energy has the same value at both minima. Following [27], the exact transition temperature kT_c may be computed by simultaneously solving $f(m) = f'(m) = 0$ and yields

$$\frac{kT_c}{\zeta(1+\sigma)} = \frac{q-2}{(q-1)\,\log(q-1)}$$

Similarly, spinodal points are computed by jointly solving $f'(m) = f''(m) = 0$, giving temperature points at which either one of the two minima vanishes. These

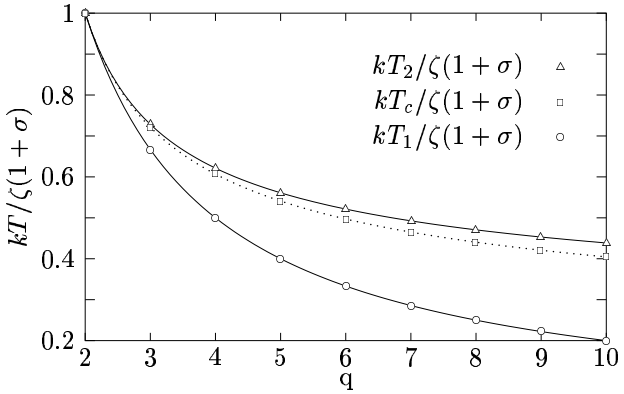

FIG. 1: Reduced temperatures of spinodal points $kT_1/\zeta(1+\sigma)$ and $kT_2/\zeta(1+\sigma)$ together with the reduced transition temperature $kT_c/\zeta(1+\sigma)$, as a function of q in the MF approximation.

equations possess one trivial solution, namely $kT_1 = 2\zeta(1+\sigma)/q$ corresponding to the extrema at $m = 0$ becoming unstable, and a non-trivial solution kT_2 which may be obtained numerically by solving the following equation,

$$\frac{K}{2}\frac{qS-2}{q-1} = \log\left(S\sqrt{\frac{Kq}{2}}\right)$$

where $S = 1 + \sqrt{1+2(1-q)/(Kq)}$ and we have set $K = \zeta(1+\sigma)/kT_2$. Alternately, one may also express f as a function of the MF energy $E = -\zeta(1+\sigma)m^2$ and impose $f'(E) = f''(E) = 0$. While these equations yield the same kT_1 and kT_2 as above, both expressions of f obviously do not have the same shape. Spinodal points are sketched in Fig. 1 for q between 2 and 10. These correspond to the limits of metastability for each subphase, respectively. For temperature points lying inside this temperature range, there exists two values of the order parameter corresponding to a zero curvature of the free energy, a feature which is known to yield a long-ranged (*i.e.* low wave-number) instability. This in turn triggers a phase transition through the so-called spinodal decomposition [37]. As expected, the width of the spinodal curve $T_2 - T_1$ shrinks to zero as $q \to 2$, and accounts for the second-order nature of the transition at $q = 2$, since in this limit the two minima merge into a single large minima responsible for the well-known divergence of fluctuations at a continuous transition.

III. THE MULTICANONICAL ALGORITHM

The Metropolis algorithm (hereafter denoted as belonging to the class of *canonical* algorithms, *i.e.* relying on a Boltzmann weighting) has long been considered the paradigm for Monte-Carlo simulations in statistical physics, yet this method faces some severe drawbacks in situations where the sequence of states created by the Markovian chain leads to very repetitive dynamics, *i.e.* dramatically low acceptance rates and exponentially diverging autocorrelation times: this makes it necessary to simulate systems over exceedingly long runs in order to obtain good statistics and reliable estimates of thermodynamical averages (see for example [38] and the contribution by Krauth in [39] for an introductory review). This is the case when one comes to simulating systems with rugged free-energy landscapes, e.g. polymers and proteins, disordered systems including spin-glasses, for the dynamics may then get trapped in one of numerous local minima, especially at low temperature. One experiences similar behavior when simulating first-order phase transition (the so-called Supercritical Slowing Down [32]), where the tunneling time between coexisting phases grows exponentially with the system size, due to the increasingly high free-energy barrier to be overcome (e.g. [40]).

Since slow dynamics mainly result from the combination of weighting the Markovian chain with Boltzmann weights and using local-updates, there have been several attempts to devise efficient update algorithms based on *global-updates*, e.g. cluster algorithms, which in the case of continuous transition decrease Critical Slowing Down by several order of magnitude (see [41, 42], also a LR implementation in [28]). On the contrary, multicanonical methods [30–32, 43] are based on random walks in energy landscape, whatever move-update is being used, whereby a *flat* energy distribution is now sampled. First, this results in the algorithm quickly sampling a much wider phase space than in the canonical case, by allowing the system to cross any free-energy barrier. Secondly, this allows the density of states to be computed over the whole energy axis, thus extending the reliability of reweighting procedures over a much wider range of temperature than in the case of standard histogram methods [44], where poor histogram sampling at low-energy usually induces strong statistical bias. As opposed to multi-histogramming [45], a single run is needed to cover the energy range of interest. Once a reliable estimate of the density of state has been obtained, it is then straightforward to compute thermodynamical functions otherwise hardly within reach of canonical simulations, e.g. canonical entropy and free-energy. It is noteworthy that this simulation technique actually belongs to a larger class of algorithms called *generalized-ensemble* algorithms, which encompass variants based on random walk in the entropic variable ("1/k-ensemble" or "entropic sampling" algorithms, [46, 47]), or the temperature variable (e.g. "simulated tempering" [48, 49]).

A. Rationale

The rationale behind the multicanonical algorithm is the generation of a Markovian chain of states $\{\sigma_i\}$, whose weights $W_{mu}(E(\sigma_i))$ are adjusted so that one eventually gets a flat energy histogram, i.e. if $P(E)$ denotes the

probability in energy, and $n(E)$ is the density of states,

$$P_{mu}(E) \propto n(E) W_{mu}(E) = const.$$

Since $n(E)$ usually increases drastically with energy, low-energy states are thus sampled much more often than high-energy ones.

Following Berg in [50], we compute $W_{mu}(E)$ through an iterative procedure, starting from an initial canonical simulation at inverse temperature β_0. β_0 indirectly sets the maximum energy value below which the energy histogram is to be flat, i.e. $E_{max} = \langle E \rangle_{\beta_0}$. Thus, $kT_0 = 1/\beta_0$ must be chosen high enough to ensure that the final energy histogram spans a sufficiently large energy range upward, e.g. reaches the energy of the disordered phase in the case of a first-order transition, and extends even further away if one wants to observe with satisfying accuracy the free-energy plateaus signaling the limit of metastability. For convenience, we now define an effective Hamiltonian $H_{mu}(E)$, so that

$$W_{mu}(E, \beta_0) = e^{-\beta_0 H_{mu}(E)}$$

Hence, multicanonical simulation can be envisioned as a canonical simulation at inverse temperature β_0 with the usual Boltzmann weight, provided the original Hamiltonian is replaced by an effective Hamiltonian to be determined iteratively. As a side note, a cluster implementation in the framework of the multicanonical algorithm is thus far less straightforward, since this effective Hamiltonian has fundamentally a global nature whereas canonical simulations explicitly preserve the locality of the original Hamiltonian (see e.g. the multibondic approach in [33, 43]).

Denoting $H^{\infty}_{mu}(E)$ as the true estimate of the effective Hamiltonian, we may thus write:

$$n(E) \propto e^{\beta_0 H^{\infty}_{mu}(E)}$$

The micro-canonical inverse temperature $\beta(E)$ may be easily related to $H^{\infty}_{mu}(E)$, as we have (assuming $k = 1$)

$$\beta(E) = \frac{d \log n(E)}{dE} = \beta_0 \frac{dH^{\infty}_{mu}(E)}{dE}$$

Since the dynamics of the Markovian chain is governed by the transition rate $W(a \rightarrow b) = min(1, \exp[\beta_0(H_{mu}(E_a) - H_{mu}(E_b))]$, we may write, for two states infinitely close in energy, *i.e.* whenever $E_b = E_a + \delta E$, $W(a \rightarrow b) = min(1, \exp[-\beta(E_a)\delta E)]$. Hence it is the **micro-canonical temperature** which is the relevant quantity where the dynamics (e.g. the acceptance rate) of the multicanonical algorithm is concerned.

B. Iteration scheme

We initially set $H^0_{mu}(E) = E$, or equivalently $\beta^0(E) = \beta_0$, as this indeed corresponds to a canonical simulation at temperature $1/\beta_0$. At step "i", a simulation is performed using a Boltzmann weight with effective Hamiltonian $H^i_{mu}(E)$, then an energy histogram $N^i(E)$ is eventually computed using independent samples. Incidentally, taking truly independent samples proves useful during the late stages of the iteration scheme only, where the aim is then to refine a nearly flat histogram. During earlier iteration steps, histograms may be computed using non-independent samples without significantly affecting the convergence. We now denote E^i_{min} as the lowest energy-value that was obtained throughout the previous runs, including step "i": this is the energy value below which $H^{i+1}_{mu}(E)$ will have to be predicted, since no histogram data is available inside this energy range. Issues regarding adequate predictor choice will be considered later on in this section. The rules for updating H^{i+1}_{mu} at step "$i+1$" from H^i_{mu} at step "i" are based on the following equations. For $E \geq E_{max}$, $H^{i+1}_{mu}(E) = E$, *i.e.* the dynamics is canonical-like at inverse temperature β_0 for all iteration steps. For $E^i_{min} \leq E < E_{max}$,

$$\beta^{i+1}(E) = \beta^i(E) + \frac{\hat{g}^i_0}{\delta E} \log \frac{N^i(E + \delta E)}{N^i(E)} \qquad (2)$$

where

$$\hat{g}^i_0 = \frac{g^i_0}{\sum_{k=1}^{i} g^k_0}$$

and g^k_0 is a *raw* inverse damping factor proportional to the reliability of the *kth* histogram. It has been shown in [50], following an error calculation argument, that

$$g_0 = \frac{N(E)N(E + \delta E)}{N(E) + N(E + \delta E)}$$

provides an estimator proportional to the inverse of the variance of $\beta^{i+1}(E)$. Once $\beta^{i+1}(E)$ is known, $H^{i+1}_{mu}(E)$ is derived by a mere integration starting from the initial condition $H_{mu}(E_{max}) = E_{max}$. Finally, for $E < E^i_{min}$, $H^{i+1}_{mu}(E)$ will have to be computed using a suitably chosen predictor, until at last E^i_{min} becomes equal to the ground-state energy. A cubic-spline is then fitted to $H_{mu}(E)$ at every bin center, and this curve is used to compute acceptance probabilities during the next run.

It can be seen that Eq. (2) leads to a steady-state whenever $N(E)$ is constant over the energy range of interest. Writing a recursion equation involving $\beta(E)$ instead of $H_{mu}(E)$ allows, together with the inclusion of a damping factor, to handle the situation where some bins have null entries, a case which otherwise leads to a fairly spiky graph for $H_{mu}(E)$ and inconsistent dynamics. *Accidental* null entries at energy values E or $E + \delta E$ will simply leave $\beta(E)$ unchanged, and the corresponding parts of $H_{mu}(E)$ thus move as a block. Since acceptance rates hinge on the microcanonical temperature, this in effect drastically reduces bias on the dynamics. Considering a small set of histogram bins that are copiously filled for the first time during a given iteration run, (e.g. high

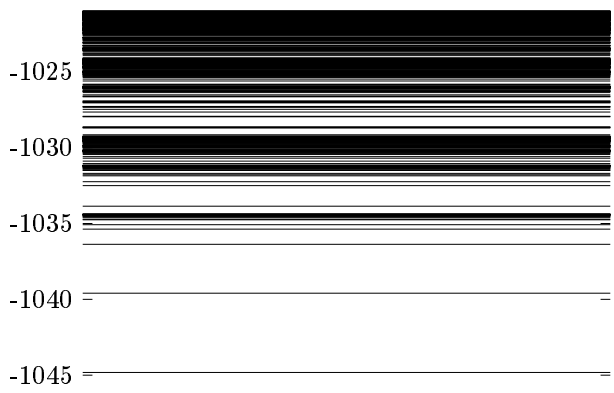

FIG. 2: Lowest energy levels for $q = 5, \sigma = 0.5, N = 400$, computed by sorting energy samples from a long simulation run.

energy bins during the early iteration runs whenever we begin with a canonical simulation), we see that the related *cumulative* inverse damping factor first soars and yield a great amount of change in $\beta(E)$ in the couple of runs that follow, then decays progressively to zero as these bins continue to be filled. By taking into account all data that have been sampled up to step i, this modified recursion both clearly stabilizes the algorithm, and reduces relative errors due to poor histogram entries.

Choosing the most appropriate value of the histogram bin width results from a trade-off between resolution and computation time. Higher resolution on the one hand guarantees a good histogram flatness, and is especially crucial at low energies, where the density of state (DOS) displays a rugged graph. On the other hand, we impose a fixed number of independent samples per histogram bin, so as to give the histogram variance an acceptable low value, hence a low δE implies more simulation steps per iteration. Our approach is thus to first choose a fairly high δE, e.g. yielding around 20 bins, in the early stages of the iteration process in order to obtain a rough picture of the density of state, then to progressively reduce δE once the ground-state energy has been reached. As will become obvious in section IV A, the ultimate value of δE deeply affects the attainable precision on the computation of spinodal points, since the latter is based on a precise location of free-energy plateaus, and this indeed entails having enough bins belonging to a given plateau. As a rule of thumb, the best compromise is then to obtain between 100 and 300 histogram bins in the final stage, with the number of bins increasing as the σ value corresponding to the second-order regime is approached.

In this view, the unequal spacing of energy levels in LR spin models deserves specific attention. As illustrated in Fig. 2, there are large energy gaps separating isolated energy levels or tiny groups thereof in the vicinity of the ground-state, whereas the distribution changes smoothly to a near continuum above $E \sim -1025$. Setting a low δE value leads in turn to *non-accidental* null entries in those bins located inside energy gaps, whereby $\beta(E)$ never gets updated at isolated energy levels for g_0 is then always zero. Since the graph of the density of state looks indeed fairly wrinkled near the ground-state, and the dynamics there is noticeably sensitive to even the smallest departure of $H_{mu}(E)$ from the ideal line, we would then observe a sharp steady peak in the lowest part of the energy histogram which the present recursion equation would not be able to suppress. One could trivially think of working this out by implementing variable-width bins that would span energy gaps. This is, however, impracticable since the distribution of energy levels is not known prior to starting the iteration process (for this is precisely what we intend to compute with the density of states). To circumvent this limitation, we have modified the previous recursion equation so that null entries are always skipped, however accidental or non-accidental they are. Denoting E_a and E_b the centers of histogram bins located on each side of a set of contiguous empty bins, with $E_a < E_b$, we have

$$\beta^{i+1}(E_a) = \beta^i(E_a) + \frac{\hat{g}_0^i(E_a)}{E_b - E_a} \log \frac{N^i(E_b)}{N^i(E_a)} \qquad (3)$$

where $\beta(E_a) = \beta_0\{H_{mu}(E_b) - H_{mu}(E_a)\}$ and we now set

$$g_0(E_a) = \frac{N(E_a)N(E_b)}{N(E_a) + N(E_b)}$$

hence g_0 can never be zero. In order to avoid loosing details of the shape of $H_{mu}(E)$ for $E_a < E < E_b$ that were possibly collected during previous runs, we update $H_{mu}(E)$ through a linear difference scheme,

$$\delta H_{mu}(E) = \frac{\delta H_{mu}(E_b) - \delta H_{mu}(E_a)}{E_b - E_a}(E - E_a) + \delta H_{mu}(E_a)$$

where $\delta H_{mu}(E) = H_{mu}^{i+1}(E) - H_{mu}^i(E)$. While this has obviously no effect where non-accidental null-entries are concerned, this favors quicker convergence during the early runs where the inadequate shape of $H_{mu}(E)$ is more likely to produce empty bins.

The iteration process stops when the energy histogram has become sufficiently flat over the energy range of interest, namely between the ground-state energy and E_{max} for our purpose. We evaluated this property by computing the standard deviation of histogram entries, as well as the same quantity for the logarithm of histogram entries restricted to non-empty bins. The latter seemed to be a better indicator since it is sensitive to both poorly populated bins and histogram peaks, whereas the former only increases with rather spiky histograms. Besides, we estimated the degree of convergence of the algorithm by computing the mean square distance between $H_{mu}^i(E)$ and $H_{mu}^{i+1}(E)$ after the ground-state energy had been reached. We then computed a threshold value for each indicator by trial and error based on a couple of short runs for various lattice sizes and bin width.

C. Reweighting procedure

Once $H_{mu}(E)$ has been satisfactorily computed, a long production run is performed using this effective Hamiltonian in place of the original one, then estimates of thermodynamical quantities of interest at inverse temperature β are computed using a reweighting scheme, *i.e.* formally,

$$\langle A\rangle_\beta = \frac{\sum_E \langle A\rangle_E n(E) e^{-\beta E}}{Z(\beta)}$$

where $\langle A\rangle_E$ denotes the microcanonical average of A at energy E, and the partition function is given by $Z = \sum_E n(E) e^{-\beta E}$. The best estimate for the density of states $n(E)$ is provided by $n(E) \propto N(E) e^{\beta_0 H_{mu}(E)}$ where $N(E)$ stands for the number of bin entries at energy E computed from the production run. In order to avoid numerical overflows, as well as to suppress bias resulting from possibly strong variance on microcanonical averages, we found it more appropriate to compute $\langle A\rangle_\beta$ from a sum running over samples instead of energy bins, *i.e.* $\langle A\rangle_\beta = \sum_i A_i w(E_i) / \sum_i w(E_i)$, where $w(E_i) = e^{\beta_0 H_{mu}(E_i) - \beta E_i - K}$. K is then determined so as to avoid both numerator and denominator overflows. Providing that the histogram sampled during the production run is flat to a good approximation, the maximum in $e^{\beta_0 H_{mu}(E) - \beta E}$ is reached when $\frac{dH_{mu}(E)}{dE} \sim \frac{\beta}{\beta_0}$. which yields the energy value at which K is to be computed. Besides, since the reweighting scheme involves exponential contribution of $H_{mu}(E)$, the resulting curve $e^{\beta_0 H_{mu}(E) - \beta E}$ is strongly peaked around the maximum, hence it is clear that only histogram points in the vicinity of this maximum contribute to $\langle A\rangle_\beta$. In effect, we found that the existence of two distinct maxima, or equivalently of two energy values for which $\beta(E)$ have the same value, coincides with the occurrence of a first-order phase transition.

Following the same reweighting procedure we compute partial free energies, *i.e.* $F(\beta, m)$ where m is the order parameter, and reweighted histogram of the energy, *i.e.* $N(\beta, E)$. The partial partition function is straightforwardly derived from a partial sum over samples having the prescribed order parameter,

$$Z(\beta, m) = \sum_i e^{\beta_0 H_{mu}(E_i) - \beta E_i} \delta_{m, m_i} \tag{4}$$

which then yields $F(\beta, m) = -\log Z(\beta, m)/\beta$. Similarly, a reweighted histogram of the energy is obtained from $N(\beta, E) = N(E) e^{\beta_0 H_{mu}(E) - \beta E}$.

D. Predictor choice

We now discuss some issues related to the choice of an efficient predictor for $E < E_{min}$. For small lattice sizes, we initially feed the algorithm with an effective Hamiltonian $H_{mu}(E) = E$, and the aim is then to find an appropriate trade-off between speeding up the convergence of E^i_{min} towards the ground-state energy and avoiding algorithm instability. While the former demands that $H^i_{mu}(E)$ has a sufficiently high slope below E^i_{min}, the latter still imposes that the algorithm remains ergodic to a sufficient extent. Our implementation relies on a first-order predictor, $H_{mu}(E) = a + bE$, and we impose continuity on $H_{mu}(E)$ at E_{min}. The simplest approach is then to choose a predictor slope so that continuity on $H'_{mu}(E)$ is enforced at $E = E_{min}$, *i.e.* $b = \beta(E_{min})/\beta_0$. While E_{min} reaches the ground-state energy rather quickly using this predictor, the dynamics often gets locked in very low energy states due to the particularly steep slope of $H_{mu}(E)$ in the vicinity of the groundstate. The time needed by the iteration scheme to recover from this deadlock and obtain a flat histogram thus becomes prohibitive. On the other hand, choosing $b = 1$ leads to the smoothest, yet slowest convergence, and avoids deadlock issues. An efficient compromise is thus to ensure a "weak" continuity at E_{min}, *i.e.* by computing the slope of the predictor using a least-square scheme based on the first ten percent of points above E_{min}.

For large lattice sizes where reaching the ground-state energy can become time-consuming, we resort to a "scaling-trick" whereby $H_{mu}(E)$ is initially guessed from the density of state obtained at a smallest lattice size. This approach was initially mentioned by Berg and Neuhaus [32], and claimed to work perfectly within the framework of a 2D 10-state Potts model with nearest-neighbor interaction where the energy is additive to a perfect extent. The presence of LR interaction, however, slightly worsens the case, especially for low σ values. The scaled density of state is computed as follows. Let us consider, for the sake of simplicity, two systems Σ et $\bar{\Sigma}$ with respective lattice sizes $L = N$ and $\bar{L} = 2N$, and let us divide the latter into two subsystems Σ_1 and Σ_2 of equal size L. Since $H_{mu}(E) = kT_0 \log n(E)$, where $n(E)$ stands for the density of states, we will have to compute $\bar{n}(E)$ for system $\bar{\Sigma}$ as a function of $n(E)$ for Σ. Neglecting interaction between subsystems Σ_1 and Σ_2, and denoting E_1 the energy of system Σ_1, the density of state for $\bar{\Sigma}$ just reads $\bar{n}(E) \simeq \sum_{E_1} n(E_1) n(E - E_1)$, which yields

$$\begin{aligned}\beta_0 \bar{H}_{mu}(E) &\simeq \log \sum_{E_1} e^{\beta_0 (H_{mu}(E_1) + H_{mu}(E - E_1))} \\ &\sim \log \frac{1}{\delta E} \int dE_1 e^{\beta_0 (H_{mu}(E_1) + H_{mu}(E - E_1))}\end{aligned}$$

where δE is the energy histogram bin width. Providing that $n(E)$ is a monotonic and rapidly increasing function of E, we may use a saddle-point approximation to evaluate the former sum. The maximum of $H_{mu}(E_1) + H_{mu}(E - E_1)$ is reached whenever $E_1 = E/2$,

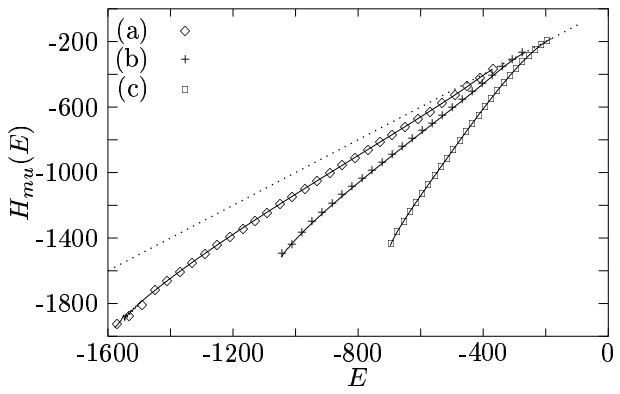

FIG. 3: Plot of initial guess $\bar{H}_{mu}(E)$ for $L = 400$ spins, computed after scaling a final estimate obtained at $L = 200$ using Eq. (5) ((a),(b),(c) refer to $q = 5, \sigma = 0.3, 0.5, 0.9$ respectively), together with a plot of $H_{mu}(E)$ as estimated after the whole iteration scheme at $L = 400$ converged (solid lines). The straight dotted line sketches the original Hamiltonian, *i.e.* $H(E) = E$.

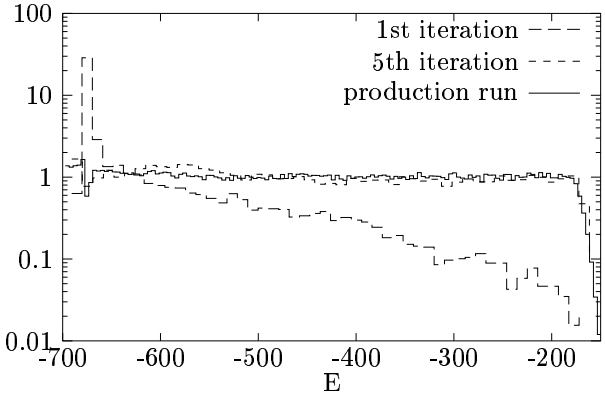

FIG. 4: Histogram of energy sampled after indicated runs, for $q = 5, \sigma = 0.9, L = 400$ spins, using Eq. (5) to compute the initial effective Hamiltonian $H_{mu}(E)$ from a previous runs at $L = 200$ spins. Labeling on y axis indicates normalized probabilities.

hence

$$\bar{H}_{mu}(E) \simeq 2H_{mu}\left(\frac{E}{2}\right) + kT_0 \log \frac{\sqrt{\pi/|H''_{mu}\left(\frac{E}{2}\right)|}}{\delta E} \quad (5)$$

This expression may be readily extended to lattice sizes being any multiple of the original size. Fig. 3 sketches results obtained for $q = 5$ and $\sigma = 0.3, 0.5$ and 0.9. A series of iteration runs was first conducted with $L = 200$ spins in order to obtain an estimate of $H_{mu}(E)$ for this lattice size, then this estimate was scaled using Eq. 5 and used as the initial guess for the next series of iterations at $L = 400$. Eq. (5) yields a very acceptable guess for $\sigma = 0.9$, and both curves are hardly distinguishable from each other. As illustrated on Fig. 4, the energy histogram becomes nearly flat within five iterations. For $\sigma = 0.3$ and 0.5, the agreement remains quite satisfying yet the initial guess falls slightly below the true estimate at low energies, and lowest energy bins are exceedingly enhanced during the first iteration runs. More and more iteration runs are thus required to obtain a perfectly flat histogram as σ is decreased, and the benefit of this approach in effect becomes negligible for $\sigma \leq 0.3$. Indeed, the algorithm then spends a great amount of iteration steps being trapped in low energy levels, trying to rectify the shape of the density of state in this energy region until convergence is obtained, and starting from an initial canonical effective Hamiltonian actually yields better performances. Since, for systems with LR interaction, computation time scales with L^2, using this "scaling trick" thus greatly reduces the time needed for proper convergence, at least for $\sigma > 0.3$, and partially compensates for the lack of a hybrid multicanonical-cluster algorithm dedicated to LR models.

E. Algorithm performance

In order to measure the performance of our implementation, we have computed a dynamical exponent z defined as the scaling exponent of a relevant characteristic time τ of the simulation, *i.e.* $\tau \propto L^z$ where L denotes the lattice size: while for second-order transitions it is widely known that the integrated autocorrelation time represents such a relevant time, for first-order transition the tunneling time through the energy barrier (τ_{tun}) turns out to be a more meaningful parameter [33]. We define the latter as one half of the average number of Monte-Carlo steps per spin (MCS) needed to travel from one peak of the energy histogram to the other. Tunneling time is expected to grow exponentially with L for canonical algorithms, and to scale as a power law of L with multicanonical algorithms [32]. In both cases, it appears that the chosen characteristic time is a good indicator of how fast needs in CPU time should grow with increasing lattice size: for second-order transition, this is the time needed to generate truly independent samples, whereas for first-order transition, this tells us at which rate the simulation spreads over the energy barrier and thus to what extent samples get efficiently picked from the two phases in coexistence.

The integrated autocorrelation time was computed by using the well-known time-displaced correlation function which displays an exponential-like short-time behavior, namely $\Phi_{mm}(t) \sim e^{-t/\tau}$; τ is then computed from a simple integration scheme. Since this latter function makes sense within equilibrium only, we first discarded n thermalization steps, where n was computed by using the non-linear relaxation function which describes the approach to equilibrium [38], and averaging over several dry-runs. An interesting point regarding multicanonical simulations is that, being random walks in energy space, "thermalization" (though this term is not appropriate anymore where generalized ensemble algorithms are concerned) always occurs rather rapidly ; simulations based

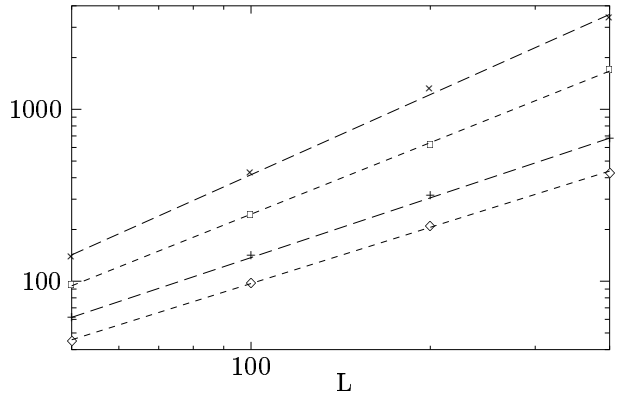

FIG. 5: Integrated autocorrelation time τ vs. lattice size L for $q = 7$ and $\sigma = 0.2, 0.4, 0.6, 0.8$ (from bottom to top). Corresponding dynamic exponents are $z = 1.09(1), 1.15(1), 1.38(1), 1.55(1)$.

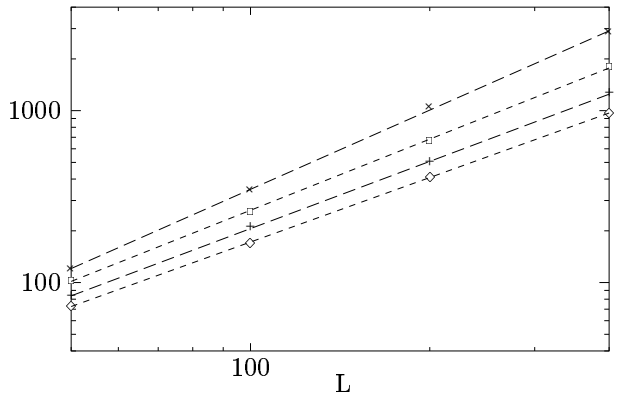

FIG. 6: Tunneling time τ_{tun} vs. lattice size L for $q = 7$ and $\sigma = 0.2, 0.4, 0.6, 0.8$. Corresponding dynamic exponents are: $z = 1.25(1), 1.30(2), 1.37(1), 1.53(1)$.

on a nearly flat histogram showed that a value of 1000 MCS was indeed appropriate in average.

Results for $q = 7$ and σ lying between 0.2 and 0.8 are shown on Fig. 5 for integrated autocorrelation times, and on Fig. 6 for tunneling times. The slight dispersion on power-law fits arises from the fact that simulations at larger sizes were conducted with a higher number of MCS steps between measurements in order to reduce memory overhead. Where computing the second indicator is concerned, this results in some tunneling events being possibly skipped, and the average tunneling time being overestimated. However, both curves show that the power-law behavior is fairly acceptable. In the case of first-order transitions, the reduction in simulation costs is thus drastic in comparison with standard canonical algorithms.

For both indicators, we obtain an average z slightly above 1 for $\sigma = 0.2$, yet z increases slightly and monotonically with decreasing range of interaction. This may be accounted for by the fact that spatial- and time-correlations grow as we depart from the MF regime and approach the SR one. As for tunneling times, the prefactor turns out to be slightly higher near the MF regime, however z increases at a lowest rate with increasing σ.

Since there are no other studies of LR models based on multicanonical algorithms, our comparison is limited to estimates obtained for SR models. For the three-state Potts model, canonical simulations using local-updates led to $z = 2.7$ [51], while Swendsen-Wang obtained $z \sim 0.6$ using their percolation cluster algorithm [41]. For further comparison, the Metropolis algorithm applied to a SR Ising chain in $d = 2$ and $d = 3$ yielded a value of z slightly above 2 [52], whereas Wolff's cluster algorithms led to $z \sim 0.27$ [53]. While our value is slightly greater than in the case of cluster implementations, it is worth underlining that our multicanonical implementation yields reliable statistics within a single MC sweep, whereas several are needed in the case of a standard canonical simulation, whatever reweighting procedure be used.

IV. NUMERICAL RESULTS

We have conducted multicanonical simulations for $q \in [3, 9]$, using for each value of q an appropriate set of σ parameters between 0.3 and 0.9, so that we would observe strong and weak first order transitions, as well as continuous ones. For $q = 3$, some simulations were performed with $\sigma > 1.0$ in order to investigate the cross-over from the LR to the SR regime. Once the density of state was determined using the iteration process described above, a production run was performed for lattice sizes between $L = 50$ and $L = 400$. The number of MC sweeps needed for each run was computed so as to yield approximately $0.5\ 10^5$ truly independent samples, which in effect restricted our work to lattice sizes $L \leq 400$.

A. Free-energy functions and FSS

As already stated in the introduction, a precise determination of the tricritical value $\sigma_c(q)$ is a real challenge, due to the weakening of the first-order transition as σ_c is approached from below. This makes traditional estimators e.g. latent heat or energy jumps fairly inefficient, since observing clear jumps in the vicinity of the tricritical value entails simulating huge lattice sizes. Glumac and Uzelac in [18] used three less traditional estimators, namely the interface free energy, the specific heat, and the reduced fourth-order Binder cumulant, which turned out to be less sensitive to this weakening: in particular, the latter quantity defined as $U_L = \langle E^4 \rangle / \langle E^2 \rangle$ is expected to reach a non-trivial constant $U_\infty \neq 1$ as $L \to \infty$ for a first-order transition only [54] ; by extrapolating $\lim_{L\to\infty} U_L$ from measures taken at different lattice sizes, they found σ_c to fall between 0.6 and 0.7 for the

three-state model. Still and all, this approach imposes simulating fairly large lattice sizes (around $L = 3000$) for the extrapolation procedure to be reliable, let alone the fact that Binder cumulants usually experience uncontrollable cross-over effects [55]. Due to the modest lattice sizes that are within reach of our local-move algorithm, we rather resort to an approach based on the location of spinodal points, which may be accurately determined already for medium lattice sizes. In contrast with multi-histogramming techniques, the multicanonical method indeed allows to obtain the partial free energy (or equally, reweighted histograms of the energy) over a range of temperature points which extends fairly away from the transition point with remarkably modest numerical effort.

The basis of our method relies on the fact that the temperature difference between both spinodal points shall tend to zero as σ_c is approached, since there are no metastable states in the case of a continuous transition. Stated differently, the condition at which metastable states occur, *i.e.* both the first and the second derivative of the partial free energy are zero, are satisfied only at the critical point for a continuous transition: hence metastable state merge into a single large minima as the transition change from first-order to second-order. Such a behavior has been widely observed indeed, e.g. for liquid-vapor transitions near the critical point, and is supported by our MF calculation.

For a given set of (q, σ) parameters, we determine the location of spinodal points by first computing a partial free energy function of the order parameter ($F(kT, m)$, see Eq. 4) over a large temperature range. Alternately, we make use of a similar function of the energy, *i.e.* $F(kT, E) = -\log H(kT, E)$, where $H(kT, E)$ denotes the reweighted histogram of the energy. While the latter function plays the same role as the partial free-energy of the magnetization, it yields a higher precision at low values of q, as we will witness in a moment. The limit of metastability at finite lattice size is then defined by $dF/dE = d^2F/dE^2 = 0$, or alternately $dF/dm = d^2F/dm^2 = 0$: for a first-order transition, this condition is met at two temperatures T_1 and T_2 which satisfy the inequality $T_1 < T_c < T_2$ where T_c denotes the transition temperature.

Since these functions usually have rather rugged graphs, we first filter out rapid oscillations with a linear smoothing filter whose order is computed so that we are left with at most three extrema over the whole temperature range of interest. By continuously varying kT within this range, we determine the temperature of each metastable state by monitoring the change in the number of minima (Fig. 7). In contrast with [18], the transition temperature $T_c(L)$ is then obtained by imposing that the total number of bin entries in $H(E)$ be the same below and above the energy corresponding to the maxima of $F(kT, E)$. This corresponds to the so-called equal-weights condition as proposed by Lee and Kosterlitz in [55], and is equivalent to the condition that the average energy be the arithmetic mean of the energy of each phase. For the sake of comparison, however, we also compute the temperature $T_{eqh}(L)$ at which both minima in $F(kT, E)$ have the same value. We then proceed with the computation of similar quantities using $F(kT, m)$, and we estimate statistical errors using a bootstrap procedure.

Graphs of reweighted histograms on Fig. 7 show that the peak and the plateau corresponding to the disordered phase are much narrower than that of the ordered phase. As a result, the precision on the determination of the temperature T_1 of the lowest metastable state is fairly lower than that of the upper metastable state (T_2). This asymmetry increases with increasing q, and in effect precludes the use of reweighted histograms for the estimation of spinodal points at $q > 7$. For $q = 9$, we thus relied on the extrema of the partial free-energy $F(kT, m)$ since this function then becomes nearly symmetric and displays peaks which are well separated. Incidentally, the asymmetric shape of $F(kT, E)$ can be accounted for by the fact that specific heats have different magnitude in the disordered and ordered phases, since this thermodynamic quantity is simply proportional to the standard deviation of the associated gaussian peak [54]. This may be readily observed by reweighting thermodynamical averages over a single phase at a time, once the maximum of $F(kT, E)$ which separates both phases has been located. Fig. 8 shows how this procedure was applied to the computation of the mean energy per spin of each subphase for $q = 3, \sigma = 0.2$ and $L = 400$ spins. A simple visual inspection allows to assess a much lower specific heat for the disordered phase than for the ordered phase.

For finite-lattice sizes however, all these temperatures experience a distinct shift proportional to the distance from the thermodynamic limit. Assuming the FSS theory developed in [54] for first-order transition to be valid in the LR case, we therefore compute infinite lattice-size temperatures by assuming power-law corrections in $1/L$. We also expect the temperature defining the limit of metastability to obey the same scaling behavior, although the double-gaussian phenomenological theory proposed in [54] does not explicitly handle this limiting case. The inclusion of a second-order term proved necessary to obtain satisfying fits, and is accounted for by the presence of small lattice sizes in our set of data. Yet interestingly enough, fitting finite-size temperatures to a power-law form $T(L) = T(\infty) + aL^b$ yields very similar extrapolated values, with discrepancies smaller than 0.1%, *i.e.* within our range of incertitude. Besides, we observed that $F(kT, E)$ and $F(kT, m)$ led to distinct finite-size shifts, with the latter easily allowing to drop second-order correction terms without much affecting the final result.

B. Transition temperatures

For the sake of completeness, we also computed transition temperatures by relying on two other estimators,

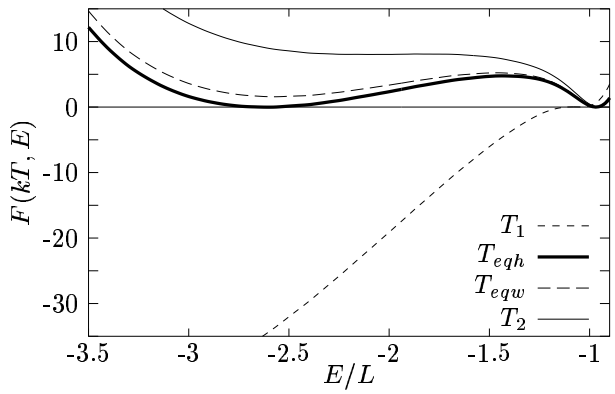

FIG. 7: Graph of $F(kT,E) = -\log H(kT,E)$ for $q = 5, \sigma = 0.3, N = 400$. E/L denotes the energy per spin. T_1, T_2, T_{eqh} and $T_{eqw} = T_c$ denote the temperatures of the two metastable states, the temperature of equal peaks heights, and that of equal peaks weights, respectively.

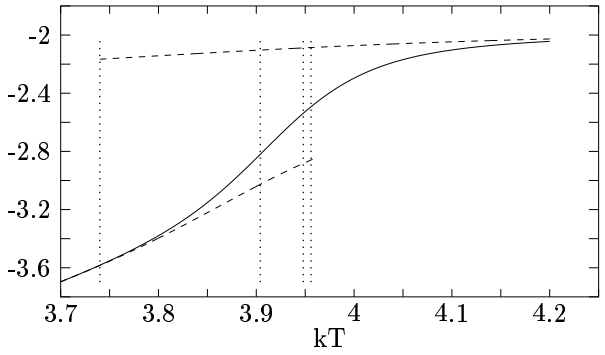

FIG. 8: Graph of the average energy per spin computed over both phases (solid line), ordered phase only (lower dashed line) and disordered phase only (upper dashed lines). Vertical dotted lines indicated the four characteristic temperatures: from left to right, lower limit of metastability, transition temperature (equal heights, then equal weights), upper limit of metastability. $q = 3, \sigma = 0.2, L = 400$

namely the magnetic susceptibility, which for magnetic systems has more pronounced peaks than the specific heat, and Binder cumulants of the magnetization defined as $U^{(4)} = 1 - \langle m^4 \rangle / (3 \langle m^2 \rangle^2)$. The latter are known to cross at a critical fixed point $U_*^{(4)}$ defining the true critical temperature, yet since crossing point drifted smoothly over our range of lattice sizes, we assumed a power law of the form L^w for $U^{(4)}(L)$, with an unknown exponent w [61]. Besides, these two quantities were advantageously used to obtain critical temperatures in the second-order regime as well (see section IV E for more details on this issue)..

Results for all temperature estimates are summarized in table I for $q = 3, 5, 7, 9$, and sketched on Fig. 9 for $q = 5$. As expected according to FSS theory, both definitions of the transition temperature, *i.e.* using equal

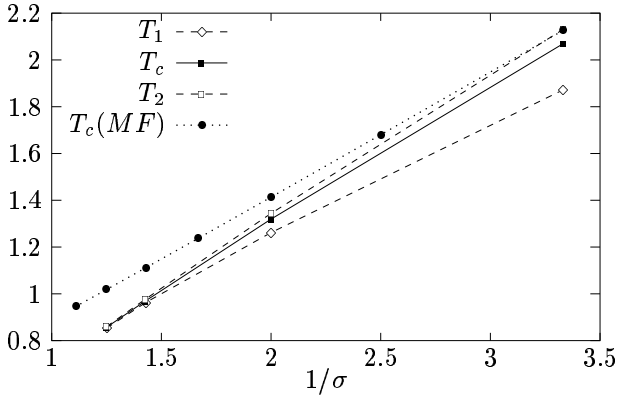

FIG. 9: Spinodal curve for $0.3 \leq \sigma \leq 0.8$ ($q = 5$). Transition temperatures T_c are indicated by the solid line, and limits of metastability T_1 and T_2 by dashed lines. Shown for completeness are MF predictions (dotted line). Lines are guide to the eyes. Error are smaller than the size of dots.

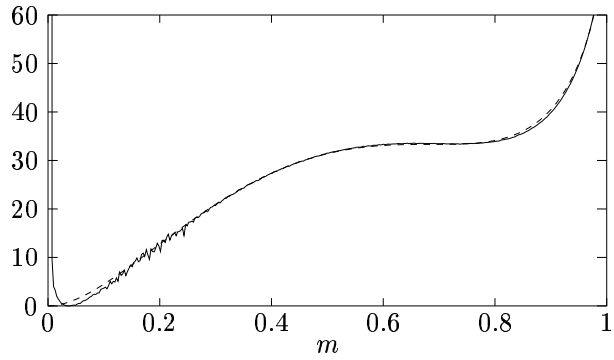

FIG. 10: Graph of $F(kT,m)$ for $q = 9, \sigma = 0.3, L = 400$ (solid line), together with the MF prediction (dashed line) as given by Eq. (1).

peaks weight vs. using equal peaks heights, lead within error bars to the same estimates at infinite lattice-size. Other quantities $T_c(\chi)$ and $T_c(U^{(4)})$ yield very similar results, with a discrepancy never exceeding 1%.

For all values of q, transition temperatures progressively departs from the MF line as σ is increased. For $q = 5$ for instance, the ratio between $T_c(\chi)$ and the MF value ranges from 97.3% at $\sigma = 0.3$ to 83.9% at $\sigma = 0.8$. We further notice that, for a given range of interaction, the adequacy with MF results is clearly improved for higher numbers of q-states. As illustrated on Fig. 10 for $q = 9, \sigma = 0.3$ and $L = 400$, this agreement also holds, even at finite lattice sizes, for the shape of the partial free-energy $F(kT,m)$ and the position of metastability plateaus. For $q = 3$ and $q = 5$, a direct comparison of transition temperatures with earlier MC studies was possible. Results obtained in [18] using the Luijten-Blöte cluster algorithm ($q = 3$) and a standard metropolis algorithm ($q = 5$) are in perfect agreement with ours within an error bar that never exceeds 1%, except in the case $\sigma = 0.2$ where our estimate lies much

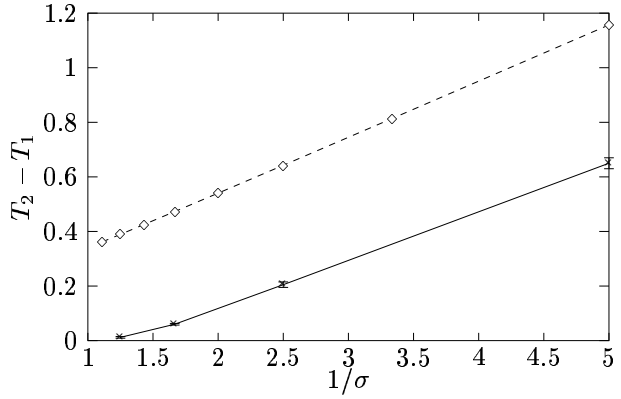

FIG. 11: $dT_m = T_1 - T_2$ vs. $1/\sigma$ for $q = 7$ (solid line). Show for comparison are MF prediction (dashed line). Lines are guide to the eyes.

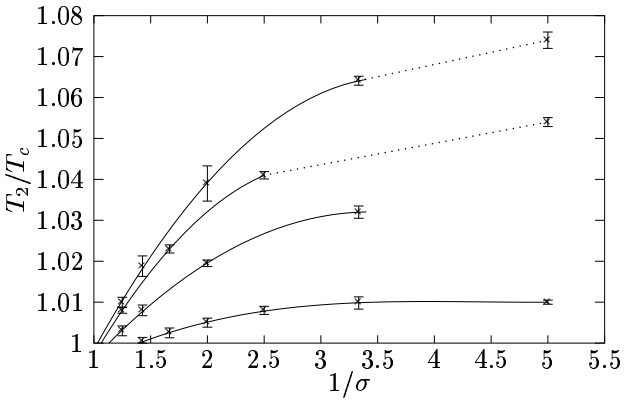

FIG. 12: T_2/T_c vs. $1/\sigma$ for $q = 3, 5, 7, 9$. Solid lines indicate polynomial fits. Dotted lines are guide to the eyes.

closer to the MF prediction. We further compared our estimates with those obtained in [14] using a Transfer Matrix approach. As illustrated in table I, results match fairly well with a discrepancy that amounts to 2% in average, except for low values of σ where the agreement of our results with MF prediction is, here again, far better.

C. Change of regime

As can be viewed on Fig. 9, spinodal points merge slightly above $\sigma \sim 0.8$ for $q = 5$, and this indeed signals the change of nature of the transition. By plotting $dT_m = T_2 - T_1$ against $1/\sigma$, we observe for all values of q that points fit quite well on a line for σ sufficient low, and the slope of this line tends towards that of the MF curve. The case $q = 7$ is sketched on Fig. 11, where it is clear that the point at $\sigma = 0.6$ marks the border between the linear and the non-linear behavior, illustrating the weakening of the first-order transition as σ_c is approached. Since these temperatures appear to scale as $1/\sigma$ in the vicinity of the MF regime, it is thus more appropriate to

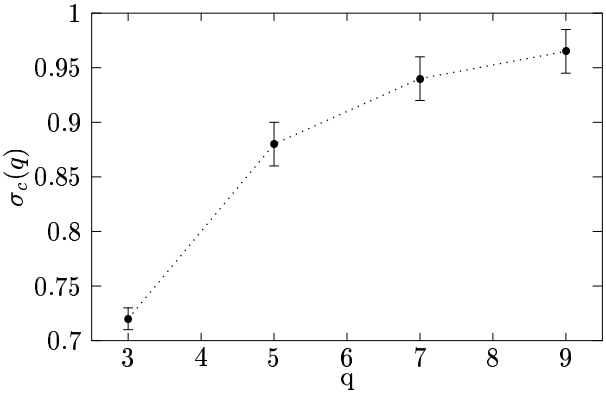

FIG. 13: Phase diagram of the LR Potts model computed using FSS properties of spinodal points. Dotted lines are shown to guide the eyes only.

work with T_1/T_c and T_2/T_c, for scaling factors shall then neatly cancel out except when approaching $\sigma_c(q)$. As mentioned above, the latter ratio offers a higher precision due to a larger free-energy plateau, and is sketched on Fig. 12. As σ falls off to the MF regime, this ratio tends, within error bars, to the values predicted by the MF theory, *i.e.* $T_2/T_c = 1.01, 1.037, 1.059, 1.077$ for $q = 3, 5, 7, 9$ respectively. On the other side of the graph, we witness a sharp decrease of T_2/T_c as $\sigma \to \sigma_c$. This brings a quite reliable way of determining $\sigma_c(q)$ without much ambiguity, as opposed to, e.g. methods using the interfacial free-energy or Binder cumulants. By fitting data points to a polynomial of degree 2 for $q = 5, 7, 9$, and of degree 3 for $q = 3$, which turned out to yield the lowest error, we obtained the following numerical estimates:

q	σ_c
3	0.72(1)
5	0.88(2)
7	0.94(2)
9	0.965(20)

Graph of $\sigma_c(q)$ is sketched on Fig. 13 for convenience. Considering the global shape of this graph, it is thus reasonable to expect $\sigma_c(q) \to 1$ as $q \to \infty$. This is clearly consistent with Cardy's scenario (as mentioned in the introduction), according to which the border case $\sigma = 1.0$ corresponds to a KT-like transition governed by topological defects, hence is incompatible with the onset of a first-order transition at $\sigma = 1.0$.

D. Unexpected FSS behavior of correlation lengths and the dynamics of first-order transitions

Let us now briefly inspect the case $q = 9, \sigma = 1.0$, where a simple analysis based on the shape of $F(kT, E)$ at a given lattice size might be markedly misleading. In [20], a first-order transition for $q \geq 9$ was reported

on the basis of the observation of a double-peaked energy histogram. We have performed a series of simulations at $L = 50, 100, 150, 200, 300$ and 400 for this set of parameters, and computed corresponding (finite-size) spinodal temperature $T_1(L)$ and $T_2(L)$ using the partial free-energy $F(kT, m)$. As may be noticed on Fig. 14, a striking feature of this limiting case is the existence of metastable states at all finite lattice sizes, with a first-order character strongly enhanced at low lattice sizes, despite the fact that FSS theory yields $T_2 - T_1 = 0$ in the thermodynamic limit. It turns out that the transition is clearly not of the first order in the the thermodynamic limit, and this feature was also confirmed for $q = 6, 7$ and 8 ; for $q < 6$, a precise location of metastable states became impracticable.

At first blush, this behavior markedly contradicts the expected picture, whereby for first-order transitions, the correlation length is finite and roughly independent of the lattice size, and is merely connected to the size of clusters. As a results, such transitions appear as if they were continuous until the lattice size overtakes the correlation length. This is thus far the standard scenario as for SR models, and we feel strongly that this scenario may be somewhat challenged, at least qualitatively to begin with, where models incorporating LR interactions are concerned.

To set the stage for an attempt to interpret this behavior, we first turn to the consequence of finite lattice-size on long wave-length fluctuations when simulating LR models with algebraically decaying interactions. The key-point in the following discussion is the nature of the phase transition as *observed* from numerical data obtained at finite-size lattices. On a lattice of size L with Periodic Boundary Conditions, the largest distance between two given spins is $L/2$, and this also corresponds to the smallest interacting potential affordable on a given lattice. It is obvious that these spins experience a stronger interacting potential when L is small, hence the whole array of spins may be rigidly tied to a sufficient extent for an order-disorder transition to occur through metastability. When increasing the lattice size on the contrary, spins distant of $L/2$ now experience a smallest interaction, and this results in a softening of the transition. Whether this softening might be sufficient to yield a change of nature of the transition at some lattice size, so that the transition may be *really* continuous in the thermodynamic limit, is however an unsettled question. Our results for $q = 9$ and $\sigma = 1.0$ in effect lend strong support to this assumption, yet only as far as FSS theory remains valid for largest sizes. Alternately, we may say that the truncation of LR interactions at small lattice sizes, whatever Periodic Boundary Conditions are used, artificially brings the model closer to the MF regime, since the interacting potential now varies smoothly with the distance over the available range.

As seems obvious to us, the usual physical meaning attributed to the correlation length in the case of SR models, *i.e.* roughly said the average size of a cluster of contiguous spins having the same value, may not hold anymore in the case of LR models: since all spins in the lattice, however distant they are, are tied together through an interacting potential, there is basically no need of a long-range order for two distant spins to have already slightly correlated fluctuations. In the framework of first-order transitions, this means that, either clusters may extend very well beyond the size permitted by the value of the correlation length, or the correlation length itself may become infinite in the thermodynamic limit. This behavior indeed has already been reported in models of DNA thermal denaturation [56] as well as in the context of wetting [57].

We have performed a couple of simulations in the first-order regime at the finite-size transition temperature, yet using a Metropolis algorithm for the associated dynamics is then closer to the real nucleation or spinodal decomposition picture than with a multicanonical algorithm. We observed indeed that clusters in the ordered phase always spanned the entire lattice, whatever the lattice size. As soon as the dynamics jumps from the disordered to the ordered phase, which we monitored by comparing the energy value with that of reweighted energy histogram peaks, a single cluster forms very rapidly and nudges its way through the crowd of disordered spins so that it swiftly occupies the whole lattice. Thus, if both phases coexist in so far as, e.g. the energy histogram has a double-peaked structure, they actually do not coexist at the same time and merely alternate in time, as opposed to what is considered the usual SR picture. In this respect, we would like to raise some challenging question regarding the dynamics of first-order transitions in the LR case: i) since both phases do not coexist at the same time, what physical meaning shall be given to the interfacial free-energy ? ii) does a mechanism similar to nucleation take place in LR system, and if in the affirmative, how shall it be reconciled with the mechanism of cluster-growth involved in SR models ?

E. Beyond the tricritical line: from LR to SR behavior

We now focus on some critical properties in the second-order regime $\sigma_c(q) < \sigma < 1.0$, then we investigate the cross-over from LR to SR behavior. As mentioned in [58], "standard" FSS theory is valid for LR systems provided the effective upper critical dimension $d^* = 2\sigma$ is greater than the geometrical dimension $d = 1$, *i.e.* $\sigma > 0.5$. Thus for $q \geq 3$ we assume "standard" finite-size scaling equations to be valid. We first determine the critical exponent ν using nth order cumulants of the magnetization, *i.e.* $V_n = d \log \langle m^n \rangle / d\beta$, which have minima obeying the scaling law $V_n^{min} \propto L^{1/\nu}$ [59]. Our approach is to compute two numerical estimates of ν by fitting reweighted averages of V_1^{min} and V_2^{min} against a power law of the lattice size, then to average over both values. Other critical exponents, *i.e.* β and γ are computed using similar

TABLE I: Estimates of the critical temperature in the first- and second-order regimes (the latter is indicated by a star): (MF) Mean-field ; (χ) Using location of peaks of the susceptibility ; ($U^{(4)}$) Using crossing points of Binder cumulants of the magnetization ; (eqw,eqh) Using the free-energy, where T_c corresponds to equal peak weights and heights, respectively ; (Ref. [18]) MC study based on multi-histogramming and the Luijten-Blöte cluster algorithm ($q = 3$) and a standard metropolis algorithm ($q = 5$) ; (Ref. [14]) Transfer Matrix method with FRS.

q	σ	T_c (MF)	$T_c(\chi)$	$T_c(U^{(4)})$	T_c(eqh)	T_c(eqw)	T_c (Ref. [18])	T_c (Ref. [14])
3	0.2	4.034	3.97(1)	3.98(1)	3.94(1)	3.97(1)	3.70[a]	3.7037
	0.3	2.836	2.72(1)	2.72(1)	2.71(1)	2.71(1)	2.70[a]	2.5907
	0.4	2.240	2.086(4)	2.089(6)	2.075(5)	2.074(4)	2.08[a]	2.0243
	0.5	1.884	1.691(3)	1.685(3)	1.686(4)	1.684(2)	1.70[a]	1.6639
	0.6	1.649	1.44(1)	1.43(1)	1.43(1)	1.43(1)	1.41[a]	1.4006
	0.7	1.482	1.196(3)	1.19(1)	1.18(1)		1.19[b]	1.1947
	0.8*	1.358	1.019(4)	1.03(1)			1.01[b]	1.0235
	0.9*	1.262	0.876	0.875			0.88[b]	0.874
5	0.3	2.127	2.07(1)	2.07(1)	2.072(6)	2.070(4)	2.033[a]	1.736
	0.5	1.413	1.321(3)	1.319(4)	1.319(3)	1.319(2)	1.297[a]	1.245
	0.7	1.111	0.973(1)	0.973(2)	0.970(3)	0.970(2)	0.981[a]	0.956
	0.8	1.018	0.854(1)	0.853(1)	0.857(1)	0.857(1)		0.844
	0.9*	0.947	0.743(2)	0.739(4)				0.745
7	0.2	2.600	2.58(1)	2.58(2)	2.578(2)	2.577(1)		
	0.4	1.444	1.395(5)	1.394(4)	1.394(1)	1.393(1)		
	0.6	1.063	0.986(2)	0.985(3)	0.984(1)	0.986(1)		
	0.8	0.875	0.764(1)	0.763(1)	0.764(1)	0.764(1)		
	0.9	0.814	0.677(1)	0.676(1)				
9	0.2	2.353	2.33(1)	2.33(1)	2.33(1)	2.32(1)		
	0.3	1.655	1.626(3)	1.625(4)	1.627(3)	1.626(1)		
	0.5	1.099	1.052(2)	1.051(2)	1.050(3)	1.052(1)		
	0.7	0.864	0.793(2)	0.792(2)	0.794(2)	0.794(1)		
	0.8	0.792	0.705(2)	0.704(1)	0.704(1)	0.704(1)		

[a]Refers to $1/K_e(\Delta F)$
[b]Refers to $1/K_e(U^{(4)})$

scaling laws, *i.e.* $M(T_c(\infty)) \propto L^{-\beta/\nu}$, and $\chi^{max} \propto L^{\gamma/\nu}$. Fig. 15 shows a power-law fit of peaks of V_1, V_2 and χ against the lattice size obtained for $q = 5, \sigma = 0.9$. Points lie neatly on a straight line when using a log-log scale, and give the following estimates: $1/\nu_1 = 0.668(2)$, $1/\nu_2 = 0.669(2), \gamma/\nu = 0.940(4)$. Error bars were computed using a bootstrap procedure. Once ν is known, we fit finite-size temperatures $T_{c,\chi}(L)$ defined from peaks of the magnetic susceptibility to a power-law of the form $T_c(L) = T_c(\infty) + \lambda L^{-1/\nu}$ and obtain an estimate of the critical temperature. As for critical couplings obtained from Binder cumulants of the magnetization, we follow the same procedure as in the first-order regime. Finally, the critical exponent β is determined by fitting $M(T_c(\infty))$ to a power law of the lattice size, and slowly varying the temperature at which M is to be sampled until the best fit is obtained. In the example considered above, this leads to $\beta/\nu = 0.103(2)$. Results for other pairs of (q, σ) values are summarized in tables I and II. For the border case $\sigma = 1.0$, exponent ratios only are shown. It can be seen that our estimates match fairly well those obtained from a previous MC study [20], and that the discrepancy with results obtained by FRS in [14] never exceed 8%. As opposed to the conjecture made in [17], the exponent ν does clearly depend on q

If the relation $\sigma = 2 - \eta$ derived in [11] is indeed exact for $q \geq 3$, we should thus observe the simple behavior $\gamma/\nu = 2 - \eta = \sigma$ in the second-order regime. As illustrated in the fifth column of table II, the qualitative behavior follows the conjecture, yet clearly $\sigma < 2 - \eta$ and the discrepancy is remarkably higher for $q = 5$ than for $q = 3$. Moreover, while it appears to shrink to 0 as $\sigma \to 1$, it is unclear whether γ/ν varies linearly with σ considering the small number of points available.

In order to get a deeper insight into the cross-over to the SR regime, we then conducted several simulations at $q = 3$ for σ above the borderline value $\sigma_{co} = 1$. This value has been reported to play the role of a critical range of interaction beyond which a crossover from LR to SR behavior sets in. According to [15, 34], $\sigma_{co} = 2 - \eta_{SR}$, where η_{SR} denotes the value of the η exponent in the SR case. Since $\gamma/\nu = 1$ for all q in the SR case, $\eta_{SR} = 1$,

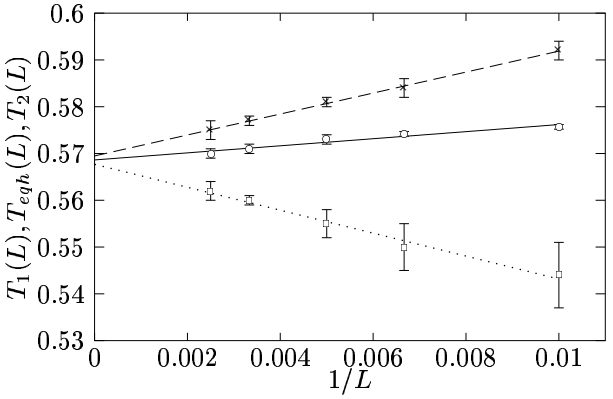

FIG. 14: Fit of finite size temperatures vs. $1/L$ for $q = 9, \sigma = 1.0$. Dotted, solid, and dashed lines correspond to T_1, T_{eqh} and T_2 respectively. In the limit $L \to \infty$, the temperature difference between both metastable states tends to 0.0012. Within our error bars, the transition is thus clearly not of the first-order.

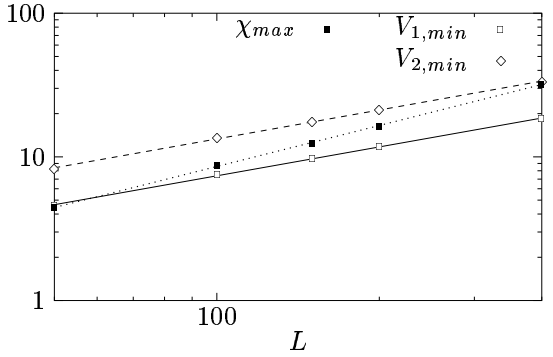

FIG. 15: Fit of $V_{1,min}$, $V_{2,min}$ and χ_{max}, vs. L on a log-log scale, for $L = 50, 100, 150, 200, 400$ ($q = 5, \sigma = 0.9$). Errors are smaller than the size of dots.

and this indeed leads to $\sigma_{co} = 1$, yet it should be noted that this definition, as initially proposed by Sak in [34] from theoretical grounding, as well as the exact location of σ_{co} within the interval $[1.0, 2.0]$, is still controversial. As shown in table II, γ/ν indeed appears to reach its SR value as $\sigma \to 1^-$, yet this ratio does not prove reliable anymore above the borderline value, as we will witness in a moment, and relying on other quantities becomes necessary.

We first review some exact results concerning the SR regime, which we obtained using a Transfer Matrix method. For $q = 3$, the transfer matrix is a 3×3 matrix having three eigenvalues, which in zero external field read $\lambda_1 = 3\cosh K - \sinh K$, $\lambda_2 = \lambda_3 = 2\sinh K$, where $K = 1/kT$. By keeping the largest eigenvalue λ_1 only, and taking the limit $L \to \infty$, we successively obtain the free-energy per spin,

$$F(K) = 1 - \frac{\log(2 + e^{2K})}{K}$$

TABLE II: Critical exponents in the second-order regime $\sigma > \sigma_c(q)$, and $q = 3, 4, 5$. Shown for comparison are results from Ref. [14] obtained using a Transfer Matrix method, and from Ref. [20] using a MC-histogram approach.

q	σ	ν^{-1}	ν^{-1} ([14])	γ/ν	β/ν
3	0.8	0.624(6)	0.574	0.842(5)	0.101(5)
	0.9	0.54(1)	0.491	0.908(5)	0.053(5)
	1.0			0.96(1)	0.025(8)
4	0.8	0.71(1)	0.67	0.882(3)	0.122(4)
	0.9	0.610(5)	0.56	0.920(4)	0.050(3)
	1.0			0.96(1)	0.022(9)
5	0.9	0.668(2)	0.62	0.940(4)	0.103(2)
	1.0			0.97(1)	0.04(1)
	1.0 ([20])			0.966	0.017

and the specific heat,

$$C_v(K) = \frac{8K^2}{\sinh K - 3\cosh K}$$

From there on, the correlation length is then computed using the standard formula $\xi = -1/\log(\lambda_2/\lambda_1)$, which then yields

$$\xi(K) = \frac{1}{\log[(3\coth K - 1)/2]}$$

Finally, the magnetic susceptibility is obtained using the fluctuation-dissipation relation, which gives

$$\chi(K) = \frac{8}{27}(1 + 2e^{2K})$$

It is then straightforward to show that $\lim_{K\to 0} \log\chi(K)/\log\xi(K) = \gamma/\nu = 1$. However, evaluating this ratio at finite temperature, *i.e.* for a finite correlation length as imposed by a finite lattice size, yields strongly overestimated results. For instance, this leads to $\gamma/\nu \sim 1.3$ for $L = 400$, a feature which is supported by our simulation results, e.g. $\gamma/\nu = 1.02(1)$, 1.14(1) and 1.23(1) for $\sigma = 1.1$, 1.5 and 4.0 respectively. Since these values are clearly overestimated, this in effect indicates the presence of exponential divergences and drastically slow convergence of correction to scaling.

This analysis was corroborated by a study of the shape of the specific heat, which turns out to provide the most tractable approach at medium lattice sizes where distinguishing between the SR and the LR regime is concerned. In the thermodynamic limit, $C_v(K)$ admits a maximum $C_v^{max} = 0.3809$ at $kT_m = 0.7534$. It is enlightening to investigate the non-monotonic behavior of this maximum at finite L, and this may be carried out by computing $F(K, L)$ then $C_v(K, l)$ while keeping all three eigenvalues. Since the calculation is fairly involved, and the final result admits no simple form, we shall hereafter simply refer to the corresponding curve sketched on Fig. 16. When L

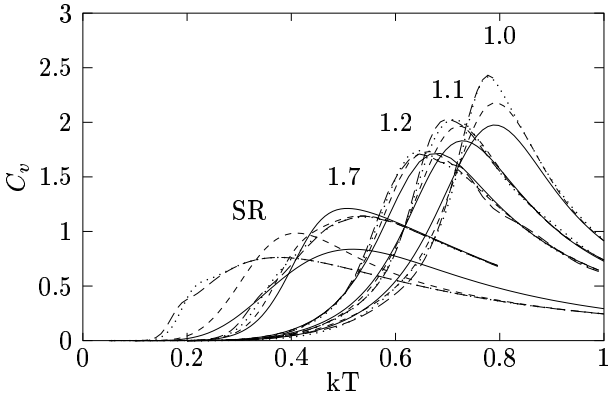

FIG. 16: Graphs of the specific heat for various lattice sizes and $\sigma = 1.0, 1.1, 1.2, 1.7$ and the pure SR case (obtained from a Transfer Matrix method), from right to left. C_v was computed using the fluctuation-dissipation relation $C_v = \langle E^2 \rangle / kT^2 / L$. Solid, dashed, dotted and long-dashed styles refer to $L = 50, 100, 200$ and 400 respectively, except for the SR case where these refer to $L = 5, 10, 100, 200$.

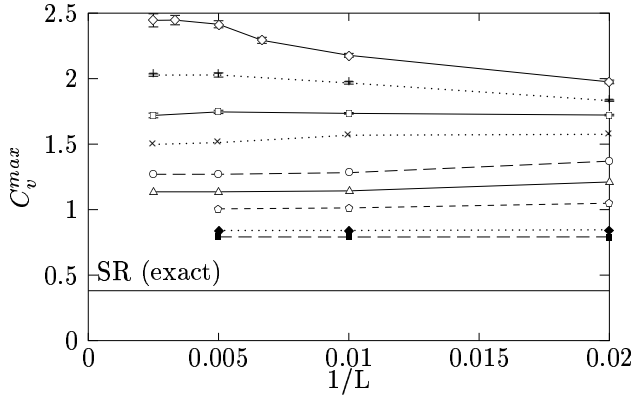

FIG. 17: Maximum of the specific heat vs. inverse lattice size for $\sigma = 1.0, 1.1, 1.2, 1.3, 1.5, 1.7, 2.0, 3.0, 4.0$ from top to bottom. The solid line is a reminder for the (exact) SR case in the thermodynamic limit. Other lines are guide to the eyes.

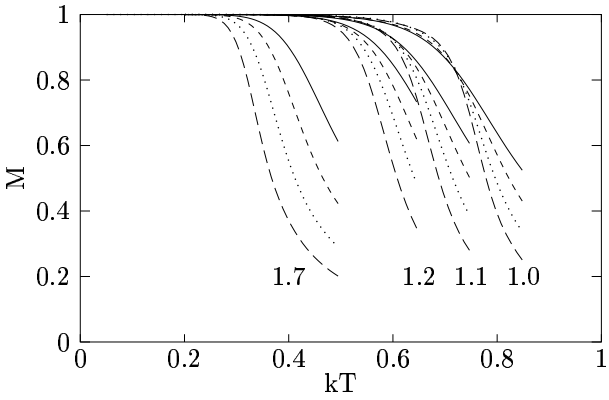

FIG. 18: Magnetization vs. kT for $\sigma = 1.0, 1.1, 1.2$ and 1.7 from right to left. Solid, dashed, dotted and long-dashed lines refer to $L = 50, 100, 200$ and 400 respectively.

is increased, the maximum of the specific heat first increases to a maximum, then graphs of C_v collapse and merge gently as the thermodynamic limit is approached. Whenever it is witnessed on reweighted numerical data, this feature thus signals a SR-like behavior.

Simulations were performed for $1.0 \leq \sigma \leq 4.0$ for various lattice sizes between $L = 50$ and $L = 400$, and we set the initial canonical temperature to $kT_0 = 1.0$ so that the maximum of C_v would be clearly visible within the whole range $\sigma \geq 1.0$. As appears obvious from a glance at Fig. 16, the cases $\sigma = 1.0$ and $\sigma = 1.1$ on the one hand, and $\sigma \geq 1.2$ on the other hand, display fairly distinct qualitative behaviors. For $\sigma = 1.0$, the specific heat reaches its maximum monotically, at least for the lattice sizes that were investigated. The slowing down in the increase rate as $1/L \to 0$ allows to assess a finite maximum in the thermodynamic limit, and this clearly shows that C_v is a nondivergent quantity, thus lending support to Cardy's scenario whereby the transition has a KT-like transition in the border case $\sigma = 1.0$. The same behavior is observed for $\sigma = 1.1$. On the contrary, the qualitative behavior is clearly different for $\sigma \geq 1.2$, where the maximum of C_v first decreases with increasing lattice size, then quickly reaches a plateau reminiscent of the exact SR behavior investigated above. While this plateau only slowly reaches the exact SR value as $\sigma \to 4.0$ (see Fig. 17), we can however conclude that the behavior is already SR-like. This assertion can be further confirmed by considering the magnetization, as sketched on Fig. 18. Graphs of this quantity clearly merge slightly above $m = 0$, whenever $\sigma \geq 1.2$, hence there is no transition at finite temperature. While for $\sigma = 1.1$, there remains some ambiguity due to statistical errors, for $\sigma = 1.0$ curve now clearly intersect around $kT \sim 0.7$, which at least shows that the behavior is not SR-like anymore. We finally computed critical temperatures from the crossing points of Binder cumulants of the magnetization. We obtained $K_c = 3.3$, 6.5 and 19 for $\sigma = 1.1$, 1.3 and 1.5. As for $\sigma = 1.7$ and $\sigma = 2.0$, cumulants do not cross anymore except at $kT = 0$ within statistical error (the latter case yielding K_c between 150 and 200, yet with excessive dispersion). While the cross-over appears to take place in the very vicinity of the critical range, the critical temperature actually dies off much slowly to 0.

All these numerical results lend support to Sak's scenario for $\sigma > 1.0$, namely that a cross-over from LR to SR behavior occurs whenever $\sigma_{co} = 2 - \eta_{SR}$. Nonetheless, it is worth mentioning that we found this cross-over to occur within the finite, yet narrow range, $1.0 < \sigma < 1.2$, and the pure SR case to be reached in the limit $\sigma \to \infty$ only. We feel strongly that this is consistent with the RG scenario of Theumann and Gusmao [15], whereby the cross-over actually results from a competition between SR and LR fixed-points. This competition, as seems obvious to us, may not resolve instantly whenever σ crosses the border case value 1.0, and may thus blur the exact

cross-over line $\sigma = 1.0$ over some finite region.

V. CONCLUSION

We have studied some critical properties of the long-ranged Potts model using a multicanonical implementation of generalized ensemble algorithms. Our implementation of the iteration procedure needed to obtain the density of state was shown to yield satisfying estimates of this quantity over a large range of energy and with much quicker and stable convergence than with the initial historical algorithm. The multicanonical algorithm allows to efficiently circumvent the slowing-down traditionally experienced in the first-order regime of spin models, and at the same time makes the reweighting approach a fairly straightforward way to examine thermodynamic quantities over a large range of temperature with strikingly modest numerical effort, *i.e.* simulating over medium lattice-sizes and performing a single long simulation run. We have used this multicanonical approach to locate spinodal points in the first-order regime over a large range of q and σ parameters. The shape of the spinodal curve in the vicinity of the change of regime then led to precise estimates of the tricritical value $\sigma_c(q)$ up to two digits. In particular, the value $\sigma_c(3) = 0.72(1)$ is perfectly consistent with the lower bound of 0.7 proposed by Krech and Luijten [23], yet in terms of precision this is markedly better by an order of magnitude. In this respect, our multicanonical implementation allows to obtain numerical results whose accuracy is at least comparable to that of previous numerical studies based on multi-histogramming and the LR cluster algorithm, although our simulations were performed on lattice having less than 400 spins. We feel strongly that this approach might be successfully applied to other spin models incorporating LR interactions, e.g. continuous spin models or frustrated systems.

Besides, our study significantly extends the range of available estimates of critical couplings and exponents. In the first-order regime, the agreement with MF predictions, and in particular with Tsallis's conjecture $T_c \sim 1/\sigma$ in the limit $\sigma \to 0$ [5], is exceptionally good. In the second-order regime, the relation $\eta = 2 - \sigma$ conjectured to be exact for $q = 2$, is shown to yield an increasingly high discrepancy when q is increased, and its validity may just be reinforced in the vicinity of $\sigma = 1$. We however found the crossover from the LR to the SR regime to take place between $\sigma = 1.0$ and $\sigma = 1.2$, thus yielding strong support to Sak's conjecture. Our detailed analysis of the case $q = 9, \sigma = 1.0$ yielded one of the most surprising result of this study, namely the unexpected behavior of correlation lengths whereby the transition appears to be of the first-order at finite lattice size despite the fact that FSS theory predicts a continuous transition in the thermodynamic limit. We feel strongly that this may be accounted for by the truncation of the LR potential, which artificially brings the model closer to the MF regime, yet we also pointed out that the physical meaning of the correlation length should be somewhat challenged in the case of LR models. The exact nature of the transition in the border case $\sigma = 1.0$, however, needs further investigation, especially at large values of q where no results have been made available thus far. In this view, an efficient combination of a global-update scheme with a multicanonical approach would be of prior importance to reach far higher lattice sizes.

Acknowledgments

S.R. is indebted to Dr. A. Revel for providing access to computing facilities at ETIS (ENSEA/UCP/CNRS) research team.

"Laboratoire de Physique Théorique et Modélisation" is associated with CNRS (UMR 8089).

[1] D.J.Amit, in *Modeling Brain Functions*, (Cambridge: Cambridge University Press, 1989).
[2] P.J.Ford, *Comtemp. Phys.*, **23**, 141 (1982).
[3] K.S.Pitzer, M.C.P. de Lima, D.R.Schreiber, *J. Phys. C: Solid State Phys.*, **89**, 1854 (1985).
[4] G.Giacomini, J.L.Lebowitz, *Phys. Rev. Lett.*, **76**, 1094 (1996).
[5] C.Tsallis, *Fractals*, **5**, 541 (1995).
[6] D.Ruelle, *Comm. Math. Phys.*, **9**, 267 (1968).
[7] D.J.Thouless, *Phys. Rev.*, **187**, 732 (1969).
[8] F.J.Dyson, *Comm. Math. Phys.*, **12**, 91 (1969).
[9] B.Simon, A.Sokal, *J. Stat. Phys.*, **25**, 679 (1981).
[10] J.Fröhlich, T.Spencer, *Comm. Math. Phys.*, **84**, 87 (1982).
[11] M.E.Fischer, S.Ma, B.G.Nickel, *Phys. Rev. Lett.*, **29**, 917 (1972).
[12] E.Luijten, H.W.J.Blöte, *Phys. Rev. Lett.*, **76**, 1557 (1996).
[13] K.Binder, E.Luijten, *Phys. Reports*, **344**, 179 (2001).
[14] Z.Glumac, K.Uzelac, *J. Phys. A*, **26**, 5267 (1993).
[15] W.K.Theumann, M.A.Gusmao, *Phys. Rev. B*, **31**, 379 (1985).
[16] J.L.Cardy, *J. Phys. A*, **14**, 1407 (1981).
[17] S.A.Cannas, A.C.N. de Magalhães, *J. Phys. A*, **30**, 3345 (1997).
[18] Z.Glumac, K.Uzelac, *Phys. Rev. E*, **58**, 4372 (1998) ; K.Uzelac, Z.Glumac, *Fizika B*, **6**, 133 (1997).
[19] Z.Glumac, K.Uzelac, *Physica A*, **271**, 147 (1999).
[20] E.Bayong, H.T.Diep, V.Dotsenko, *Phys. Rev. Letter*, **83**, 14 (1999).
[21] J.L.Monroe, *J. Phys. A*, **32**, 7803 (1999).
[22] K.Uzelac, Z.Glumac, *Phys. Rev. Lett.*, **85**, 5255 (2000).
[23] M.Krech, E.Luijten, *Phys. Rev. E*, **61**, 2058 (2000).
[24] E.Luijten, H.Messingfeld, *Phys. Rev. Lett.*, **86**, 5305 (2001).
[25] A.Aharony, E.Pytte, *Phys. Rev. B*, **23**, 362 (1981).

[26] R.J.Baxter, *J. Phys. C*, **6**, L445 (1973)?
[27] F.Y.Wu, *Rev. Mod. Phys.*, **54**, 235 (1982).
[28] E.Luiten, H.W.J.Blöte, *Int. J. Mod. Phys. C*, **6**, 359 (1995).
[29] J.M.Kosterlitz, *J. Phys. C:Solid State Phys.*, **7**, 1046 (1974).
[30] B.A.Berg, T.Neuhaus, *Phys. Lett.*, **B267**, 249 (1991).
[31] B.A.Berg, *Int. J. Mod. Phys.*, **C3**,1083 (1992).
[32] B.A.Berg, T.Neuhaus, *Phys. Rev. Lett.*, **68**, 9 (1992).
[33] W.Janke, S.Kappler, *Nucl. Phys. B*, **B42**, 876 (1995); W.Janke, S.Kappler, *Phys. Rev. Lett.*, **74**, 212 (1995).
[34] J.Sak, *Phys. Rev. B*, **8**, 281 (1973).
[35] M.J.Wragg, G.A.Gehring, *J. Phys. A*, **23**, 2157 (1990).
[36] P.M.Chaikin, T.C.Lubensky, in *Principles of condensed matter physics*, (Cambridge: Cambridge University Press, 1995).
[37] J.D.Gunton, M. San Miguel and P.S. Sahni, The dynamics of first-order phase transitions, in: *Phase transitions and critical phenomena, Vol.8*, C.Domb and J.L.Lebowitz editors (Academic Press, New-York, 1989).
[38] D.P.Landau, K.Binder, A guide to Monte Carlo simulations in statistical physics (Cambridge University Press, 2000).
[39] H.Flyvbjerg, *Advances in Computer Simulation*, Lectures Held at the Eötvös Summer School in Budapest, Hungary, 16-20 July 1996, edited by J.Kertész & I.Kondor (Springer, 1998).
[40] K.Binder, *Phys. Rev. A*, **25**, 1699 (1982).
[41] R.H.Swendsen, J-S. Wang, *Phys. Rev. Lett.*, **58**, 86 (1987).
[42] U.Wolff, *Phys. Rev. Lett.*, **62**, 361 (1989).
[43] W.Janke, *Physica A*, **254**, 164 (1998).
[44] A.M.Ferrenberg and R.H.Swendsen, *Phys. Rev. Lett.*, **61**, 2635 (1988).
[45] A.M.Ferrenberg and R.H.Swendsen, *Phys. Rev. Lett.*, **63**, 1195 and 1658 (1989).
[46] J.Lee, *Phys. Rev. Lett.*, **71**, 211 (1993); *Phys. Rev. Lett.*, **71**, 2353(E) (1993).
[47] B.Hesselbo, R.B. Stinchcombe, *Phys. Rev. Lett.*, **74**, 2151 (1995).
[48] E.Marinari, G.Parisi, *Europhys. Lett.*, **19**, 451 (1992).
[49] A.P.Lyubartsev, A.A.Martinovsky, S.V.Shevkunov, P.N.Vorontsov-Velyaminov, *J. Chem. Phys.*, **96**, 1776 (1992).
[50] B.A.Berg, *J. Stat. Phys.*, **82**, 323 (1996); B.A.Berg, *Fields Inst.Commun.*, **26**, 1 (2000).
[51] J.K.Williams, *J. Phys. A*, **18**, 49 (1985).
[52] S.Wansleben, D.P.Landau, *Phys. Rev. B*, **43**, (1991) 6006.
[53] U.Wolff, *Phys. Lett. A*, **228**, 379 (1989).
[54] M.S.S. Challa, D.P.Landau, K.Binder, *Phys. Rev. B*, **34**, 1841 (1986).
[55] J.Lee, J.M.Kosterlitz, *Phys. Rev. Lett.*, **65**, 137 (1990).
[56] N. Theodorakopoulos, T. Dauxois, M. Peyrard, *Phys. Rev. Lett.*, **85**, 6 (2000).
[57] V.Privman, N.M.Švrakić, *Phys. Rev. B*, **37**, 5974 (1988).
[58] E.Luijten, H.W.J.Blöte, *Phys. Rev. B*, **56**, 8945 (1997).
[59] A.M.Ferrenberg, D.P.Landau, *Phys. Rev. B*, **44**, 5081 (1991).
[60] C.Holm, W.Janke, *J. Phys. A*, **27** 2553 (1994).
[61] K.Binder, *Z. Phys. B*, **43**, 119 (1981); K.Binder, *Phys. Rev. Lett.*, **47**, 693 (1981).